Final version of this paper was published at
IEEE Transactions on Industry Applications. 2022, 2022 7847-7856 DOI: 10.1109/TIA.2022.3198625

A Linear Eddy Current Speed Sensor for Speed Measurement of Conductive Objects

Mehran Mirzaei, *Senior Member, IEEE*, Pavel Ripka, *Member, IEEE*,
and Vaclav Grim, *Member, IEEE*

***Abstract*—This paper presents the novel structure of an eddy current sensor for linear speed measurements. The sensor has one excitation coil and two pairs of antiserially connected pick-up coils, which are located inside and outside the excitation coil. The design and modeling of the sensor are considered with an air core and with a magnetic yoke (core) to compare their performances in terms of sensitivity and nonlinearity error. The experiments and the analysis are performed at different excitation frequencies and speeds. A novel 3D analytical method is developed and utilized for parametric analysis and for the design of this sensor. The simulation results are compared with measurements up to 16.7 m/s (60 km/h). The achieved nonlinearity error is as low as 0.3%.**

***Index Terms*—Analytical, component, conductive, eddy current, speed sensor, measurements.**

NOMENCLATURE

N_e	Number of turns in the excitation coil
$N_{p,1,2}$	Number of turns in each pick-up coil
d	Moving part thickness
g_m	Gap between coils and moving part
g_y	Gap between coils and magnetic yoke
t_y	Magnetic yoke thickness
t_e	Thickness of excitation coil
$t_{p,1,2}$	Thickness of each pick-up coil
h_e	Height of excitation coil
$h_{p,1,2}$	Height of each pick-up coil
w_{el}	Inner longitudinal width of the excitation coil
w_{et}	Inner transversal width of the excitation coil
$w_{pl,1}$	Inner longitudinal width of pick-up coils, 1
$w_{pt,1}$	Inner transversal width of pick-up coils, 1
$w_{pl,2}$	Inner longitudinal width of pick-up coils, 2
$w_{pt,2}$	Inner transversal width of pick-up coils, 2
r_{ds}	Distance between centers of sensor and disk
σ_y	Electrical conductivity of the magnetic yoke
σ_m	Electrical conductivity of the moving part
$\mu_{r,y}$	Relative magnetic permeability of the magnetic yoke
$\mu_{r,m}$	Relative magnetic permeability of the moving part
f	Frequency
V	The speed of the moving part
l	The length of the analytical model in the x-direction
L	The width of the analytical model in the z-direction
m, n	Space harmonic orders – odd numbers
I	Applied current - rms value
A_x	x - component of the magnetic vector potential
A_z	z - component of the magnetic vector potential
H_x	x - component of the magnetic field strength
J_x	x - component of the current density
J_z	z - component of the current density
U_p	The induced voltage in the pick up coils
$\Psi_{p,d}$	The difference of the mutual flux linkage

I. INTRODUCTION

Speed measurements are a vital issue for various applications, for example, railways and transportation. Rotational speed sensors with variable reluctance and optical configurations are traditional approaches for indirect speed measurements in railways, but these methods are sensitive to slip [1]-[2]. Accurate true linear speed measurements and estimates are critical for high-efficiency operation and minimum losses in transportation systems [3]-[4]. Linear speed sensors with tachometers, Hall-effect based sensors, microwave Doppler radar [5], accelerometers, GPS [6] and correlation methods using two sensors [7]-[9] are alternative devices for direct and indirect speed measurements in railway applications. Doppler radar is subject to angular error [5], while GPS is not available in tunnels. A linear resolver using a permanent magnet was used for precise positioning and speed measurements in [10]. However, it has bulky windings with less fault-tolerant characteristics. Utilizing eddy currents is a known method for measuring speed and position [8]-[9], [11]. A velocity estimation method using eddy currents within magnetostrictive position sensors was presented in [12], but this approach is not feasible for railway and high-speed applications.

The sensorless method could be also utilized for speed estimation [13], which is not reliable at fault conditions in the electrical propulsion systems.

Conventional methodologies for measuring linear speeds can be less effective for advanced types of transportation systems, because of the complicated infrastructure that is required [14]-[16]. A new method for making speed measurements using moving permanent cylinder magnets was presented in [17]. In order to improve fault tolerance, however, it is preferable to avoid having a moving component in the speed sensor.

The motional component of eddy currents in conductive metallic parts is induced when the moving part has the relative speed to the source fields [18] - [21]. Utilizing the motion-induced eddy current in the conductive part is an appropriate technique for measuring linear speed, especially at high speeds [22]. The voltages induced in pick-up coils moving with respect to the conducting target were used as speed meters.

Final version of this paper was published at
IEEE Transactions on Industry Applications. 2022, 2022 7847-7856 DOI: 10.1109/TIA.2022.3198625

The authors developed and measured parallel-type and perpendicular-type linear eddy current speed sensors [1], [23]-[26] for transportation. The eddy current speed sensors presented in [23]-[25] have only one pair of antiserially pick up coils. Only one pick up coil was used in presented sensor in [26], which is located perpendicularly to the excitation coil of the sensor. The speed sensor presented in [23] was evaluated at the speed range below 2 m/s and it was considered without magnetic yoke and shield. The sensitivity of the sensor was increased in [24] using magnetic yoke and shield and it was operated at the speed range up to 12 m/s. The sensitivity of the eddy current speed sensor was further improved using ferrite core and higher number of turns in the coils in [25]. All presented eddy current speed sensors were only operated and analyzed up to maximum speed of 54 km/h in [23]-[26]. Using just one pick up coil or one pair of pick up coils makes the speed sensor to be less fault tolerant.

A novel parallel-type eddy current sensor with a magnetic yoke is presented in this paper, with two pairs of pick-up coils for measurements of the voltage caused by motion-induced eddy currents in the moving conductive parts. The proposed eddy current sensor has higher sensitivities in both pairs of pick-up coils in comparison with the sensor in [1]. For example, the novel structure of the proposed sensor causes its sensitivity corresponding to the second pair of pick-up coils to increase over 20 times in comparison with the sensor presented in [1]. A novel 3D analytical method has been developed and used for simulations, analysis and the design of an eddy current speed sensor. Using the developed analytical method helps for exact modeling, performing of parametric analyses and fast design optimization of the eddy current speed sensor. The sensor performance was measured and analyzed with and without magnetic yoke. Iron and aluminum plates are considered as the moving parts. The performance evaluating of the eddy current speed sensor at higher speeds up to 1225 km/h is also evaluated and presented.

II. Structure and Performance Theory of The Sensor

A 3D model of a linear eddy current speed sensor with a moving part is shown in Fig. 1. It shows one excitation coil and two pairs or sets of pick-up coils parallel to the conductive moving part. The pick-up coils in each pair are connected antiserially for the voltage measurement caused by the speed of the conductive moving part, which is used as a speed meter. Speed measurements are performed utilizing the voltage of the pick-up coils, see Fig. 1. The induced differential voltage is zero in antiserially connected pick-up coils at zero speed, as the magnetic flux is symmetric and the flux linkages are equal in the two pick-up coils. The induced differential voltage is not zero at nonzero speed because the flux linkages are unequal, due to the asymmetric magnetic flux caused by the motional component of the induced eddy current in the moving part.

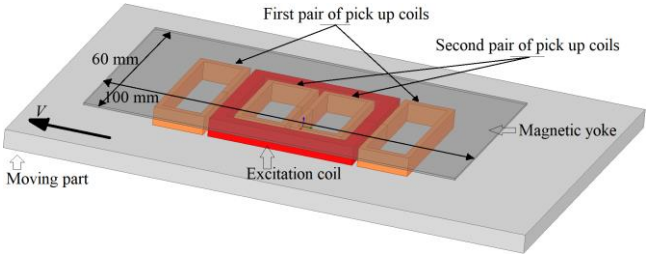

Fig. 1. A 3D model of the eddy current speed sensor and the moving part

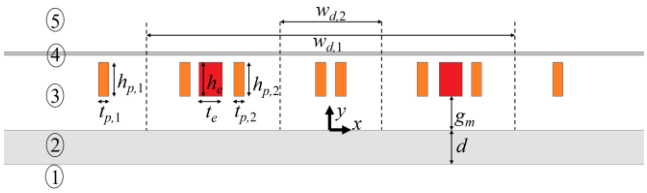

Fig. 2. A 2D model of the eddy current speed sensor and the moving part in a *y-x* model

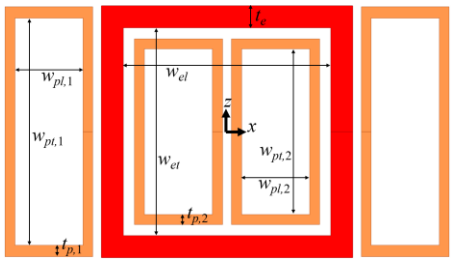

Fig. 3. A 2D model of the eddy current speed sensor in a *z-x* model

III. 3D Analytical Method for The Sensor Analysis

A 3D model is considered for analytical modeling. 2D views of the model in the *y-x* and *z-x* planes are shown in Fig. 2 and Fig. 3. The magnetic yoke is 100 mm in longitudinal length and 60 mm in transversal width, as shown in Fig. 1. However, they are artificially considered with a larger value to simplify the boundary conditions in analytical modeling. The dimensions and parameters of the sensor are presented in Table I. The proposed analytical method is used for the parametric and sensor performance analyses. The evaluation of the sensor at higher speeds, V > 600 km/h is also considered in this paper using analytical method. The analytical method could be used for design optimization of the eddy current speed sensor too, which is out of the scope of this paper.

TABLE I
Parameters and Dimensions of the Eddy Current Speed Sensor

Parameter	Value	Parameter	Value
N_e	200	$h_{p,\,1,\,2}$	5 mm
$N_{p,\,1,\,2}$	100	w_{el}	32 mm
d	5 mm	w_{et}	32 mm
g_m	6, 8 mm	$w_{pl,1}$	10.5 mm
g_y	1 mm	$w_{pt,1}$	35 mm
t_y	0.5 mm	$w_{pl,2}$	10.5 mm
t_e	3.4 mm	$w_{pt,2}$	25.5 mm
$t_{p,\,1,\,2}$	1.7 mm	$w_{d,1}$	55 mm
h_e	5 mm	$w_{d,2}$	15 mm

A. Analytical Modeling of The Sensor

Only the reaction fields of the induced eddy current in the

Final version of this paper was published at
IEEE Transactions on Industry Applications. 2022, 2022 7847-7856 DOI: 10.1109/TIA.2022.3198625

conductive part contribute to the induced voltage of antiserially connected pick-up coils [23]. The excitation coil is therefore excluded in the modeling, and the excitation fields are considered by the boundary conditions.

The *x* and *z* components of the magnetic vector potential, A_x and A_z, are considered in the analytical modeling, as the current direction in the excitation coil is in parallel with the conductive moving part or the *z*-*x* plane, and the *y* component of the magnetic vector potential, A_y, is neglected.

A Coulomb gauge is used for gauging to obtain a unique solution [27], and it does not include the electrical scalar potential in the formulation.

$$\nabla \cdot A = 0 \rightarrow \frac{\partial A_x}{\partial x} + \frac{\partial A_z}{\partial z} = 0 \tag{1}$$

Equation (2) presents partial differential equations for 5 regions, as shown in Fig. 2, versus A_z as the *z*-component of the magnetic vector potential. Similar differential equations are also valid for the *x*-component of the magnetic vector potential, A_x, using (1). Regions 1, 2, 3, 4, and 5 correspond to the parts below the moving part, the moving part, the air gap between the coils and the moving part, the coils, the air gap between the magnetic yoke and the coils, the magnetic yoke and air region above the magnetic yoke, respectively. The conductive moving parts are made of solid aluminum and solid iron.

$$\begin{gathered}
\frac{\partial^2 A_{z,1}}{\partial x^2} + \frac{\partial^2 A_{z,1}}{\partial y^2} + \frac{\partial^2 A_{z,1}}{\partial z^2} = 0 \\
\frac{\partial^2 A_{z,2}}{\partial x^2} + \frac{\partial^2 A_{z,2}}{\partial y^2} + \frac{\partial^2 A_{z,2}}{\partial z^2} = \sigma_m \mu_0 \mu_{r,m} \left(j\omega A_{z,2} + V \frac{\partial A_{z,2}}{\partial x} \right) \\
\frac{\partial^2 A_{z,3}}{\partial x^2} + \frac{\partial^2 A_{z,3}}{\partial y^2} + \frac{\partial^2 A_{z,3}}{\partial z^2} = 0 \\
\frac{\partial^2 A_{z,4}}{\partial x^2} + \frac{\partial^2 A_{z,4}}{\partial y^2} + \frac{\partial^2 A_{z,4}}{\partial z^2} = j\omega \sigma_y \mu_0 \mu_{r,y} A_{z,4} \,, \omega = 2\pi f \\
\frac{\partial^2 A_{z,5}}{\partial x^2} + \frac{\partial^2 A_{z,5}}{\partial y^2} + \frac{\partial^2 A_{z,5}}{\partial z^2} = 0
\end{gathered} \tag{2}$$

The separation of variables method is used to solve the partial differential equations in (2). The assumptions are that the magnetic fields are a sinusoidal function versus time, $e^{j\omega t}$, and the periodical sinus series functions in *x* and *z* directions with $2l$ and $2L$ periods, as presented in (3). Parameters l and L correspond to the boundaries, where zero magnetic fields can be applied. Equation (1) was rewritten for each harmonic order in (4).

$$\begin{gathered}
A_z = \sum_m \sum_n A_z^{m,n}, \;\; A_z^{m,n} \propto e^{j(\omega t - px - qz)} \\
\frac{\partial A_z^{m,n}}{\partial x} = -jpA_z^{m,n}, \quad p = m\frac{\pi}{l}, m = \pm 1, \pm 3, \cdots \\
\frac{\partial A_z^{m,n}}{\partial z} = -jqA_z^{m,n}, \quad q = n\frac{\pi}{L}, n = \pm 1, \pm 3, \cdots
\end{gathered} \tag{3}$$

$$pA_x^{m,n} + qA_z^{m,n} = 0 \tag{4}$$

The solutions of (2) are obtained using separation of variables (Fourier method) [27], as follows:

$$\begin{gathered}
A_{z,1} = \sum_{m=\pm 1,\pm 3,\cdots} \sum_{n=\pm 1,\pm 3,\cdots} \left(C_{1,1} e^{\gamma y} + C_{2,1} e^{-\gamma y} \right) e^{j(\omega t - px - qz)} \\
\gamma = \sqrt{p^2 + q^2} \\
A_{z,2} = \sum_{m=\pm 1,\pm 3,\cdots} \sum_{n=\pm 1,\pm 3,\cdots} \left(C_{1,2} e^{\lambda_c y} + C_{2,2} e^{-\lambda_c y} \right) e^{j(\omega t - px - qz)} \\
\gamma_c = \sqrt{\gamma^2 + j(\omega - mV)\sigma_m \mu_0 \mu_{r,m}} \\
A_{z,3} = \sum_{m=\pm 1,\pm 3,\cdots} \sum_{n=\pm 1,\pm 3,\cdots} \left(C_{1,3} e^{\gamma y} + C_{2,3} e^{-\gamma y} \right) e^{j(\omega t - px - qz)} \\
A_{z,4} = \sum_{m=\pm 1,\pm 3,\cdots} \sum_{n=\pm 1,\pm 3,\cdots} \left(C_{1,4} e^{\lambda_s y} + C_{2,4} e^{-\lambda_s y} \right) e^{j(\omega t - px - qz)} \\
\gamma_s = \sqrt{\gamma^2 + j\omega \sigma_y \mu_0 \mu_{r,y}} \\
A_{z,5} = \sum_{m=\pm 1,\pm 3,\cdots} \sum_{n=\pm 1,\pm 3,\cdots} \left(C_{1,5} e^{\gamma y} + C_{2,5} e^{-\gamma y} \right) e^{j(\omega t - px - qz)}
\end{gathered} \tag{5}$$

In order to obtain constants C_1's and C_2's in (5), the boundary conditions in (6) between regions are applied [23] and [27], using the magnetic vector potential, A_z, and the *x*-component of the magnetic field strength, H_x, in 5 regions (Fig. 2).

$$\begin{gathered}
A_{z,1} = 0\big|_{y=-\infty} \\
H_{x,1} = H_{x,2}\big|_{y=-d} \\
A_{z,1} = A_{z,2}\big|_{y=-d} \\
H_{x,2} = H_{x,3} + H_{x,b}\big|_{y=0} \\
A_{z,2} = A_{z,3} + A_{z,b}\big|_{y=0} \\
H_{x,3} + H_{x,u} = H_{x,4}\big|_{y=g_m+h_e+g_y} \\
A_{z,3} + A_{z,u} = A_{z,4}\big|_{y=g_m+h_e+g_y} \\
H_{x,4} = H_{x,5}\big|_{y=g_m+h_e+g_y+t_y} \\
A_{z,4} = A_{z,5}\big|_{y=g_m+h_e+g_y+t_y} \\
A_{z,5} = 0\big|_{y=\infty}
\end{gathered} \tag{6}$$

where, $A_{z,b}$, $A_{z,u}$, $H_{x,b}$ and $H_{x,u}$ are the magnetic vector potential and the magnetic field strengths, which correspond to the excitation coils [23] for applied current rms value, I, as follows:

$$\begin{gathered}
A_{z,b}^{m,n} = \frac{\mu_0 J_s^{m,n}}{\gamma^2} e^{-\gamma\left(g_m + \frac{h_e}{2}\right)} \sinh\left(\gamma \frac{h_e}{2}\right) \\
H_{x,b}^{m,n} = \gamma \cdot A_{z,b}^{m,n}
\end{gathered}$$

Final version of this paper was published at
IEEE Transactions on Industry Applications. 2022, 2022 7847-7856 DOI: 10.1109/TIA.2022.3198625

$$A_{z,u}^{m,n} = \frac{\mu_0 J_s^{m,n}}{\gamma^2} e^{-\gamma\left(g_s+\frac{h_e}{2}\right)} \sinh\left(\gamma \frac{h_e}{2}\right)$$
$$H_{x,u}^{m,n} = -\gamma \cdot A_{z,u}^{m,n} \quad (7)$$

$$J_s^{m,n} = C_e \cdot \frac{N_e \cdot I}{h_e \cdot t_e}$$
$$C_e = 4\frac{j}{n\pi l} \cdot \left(\frac{1}{p+q} C_{e,1} - \frac{1}{p-q} C_{e,2}\right)$$
$$C_{e,1} = \cos\left(p\frac{w_{el}+t_e}{2} + q\frac{w_{et}+t_e}{2}\right) \sin\left(p\frac{t_e}{2} + q\frac{t_e}{2}\right)$$
$$C_{e,2} = \cos\left(p\frac{w_{el}+t_e}{2} - q\frac{w_{et}+t_e}{2}\right) \sin\left(p\frac{t_e}{2} - q\frac{t_e}{2}\right) \quad (8)$$

The induced voltages U_p are calculated in (9) for the first and second pairs of antiserially connected pick-up coils. $\Psi_{p,d}$ is the difference of the mutual flux linkage between the excitation coil and each pick-up coil in each pair, which is averaged over the cross-sectional area of the pick-up coils. Line integration of the magnetic vector potentials, $A_{x,z,3}$, is applied to the pick-up coils regions in the artificial current flow direction (the *x*-*z* plane), as in the case of the excitation coil. $U_{p,1}$ and $U_{p,2}$ are the differential induced voltages in the first and second pairs of pick-up coils, which are presented in (10) using the parameters in (11), (12) and (13).

$$U_p = -j\omega\Psi_{p,d}\,, \qquad \Psi_{p,d} = \frac{N_p \int\int A_{x,z,3} \cdot dl\, ds}{h_p \cdot t_p} \quad (9)$$

$$U_{p,1} = -2\omega \frac{N_{p,1} \cdot L \cdot l}{h_{p,1} \cdot t_{p,1}} \sum_m \sum_n \left(1 + \frac{q^2}{p^2}\right) U_0^{m,n} C_{p,1} \cdot \sin\left(p\frac{w_{d,1}}{2}\right)$$
$$U_{p,2} = -2\omega \frac{N_{p,2} \cdot L \cdot l}{h_{p,2} \cdot t_{p,2}} \sum_m \sum_n \left(1 + \frac{q^2}{p^2}\right) U_0^{m,n} C_{p,2} \cdot \sin\left(p\frac{w_{d,2}}{2}\right) \quad (10)$$

$$C_{p,1} = 4\frac{j}{n\pi l} \cdot \left(\frac{1}{p+q} C_{p,1,1} - \frac{1}{p-q} C_{p,1,2}\right)$$
$$C_{p,1,1} = \cos\left(p\frac{w_{pl,1}}{2} + q\frac{w_{pt,1}}{2} + (p+q)\frac{t_{p,1}}{2}\right) \sin\left((p+q)\frac{t_{p,1}}{2}\right)$$
$$C_{p,1,2} = \cos\left(p\frac{w_{pl,1}}{2} - q\frac{w_{pt,1}}{2} + (p-q)\frac{t_{p,1}}{2}\right) \sin\left((p-q)\frac{t_{p,1}}{2}\right) \quad (11)$$
$$C_{p,2} = 4\frac{j}{n\pi l} \cdot \left(\frac{1}{p+q} C_{p,2,1} - \frac{1}{p-q} C_{p,2,2}\right)$$
$$C_{p,2,1} = \cos\left(p\frac{w_{pl,2}}{2} + q\frac{w_{pt,2}}{2} + (p+q)\frac{t_{p,2}}{2}\right) \sin\left((p+q)\frac{t_{p,2}}{2}\right)$$
$$C_{p,2,2} = \cos\left(p\frac{w_{pl,2}}{2} - q\frac{w_{pt,2}}{2} + (p-q)\frac{t_{p,2}}{2}\right) \sin\left((p-q)\frac{t_{p,2}}{2}\right) \quad (12)$$

$$U_0^{m,n} = \frac{C_{1,3}}{\gamma}\left(e^{\gamma(g_m+h_{p,1,2})} - e^{\gamma g_m}\right) - \frac{C_{2,3}}{\gamma}\left(e^{-\gamma(g_m+h_{p,1,2})} - e^{-\gamma g_m}\right) \quad (13)$$

Parameters l and L in (3) for Fourier method analysis are considered large enough until the magnetic fields vanish. They are calculated about 1420 mm and 100 mm in this paper, according to the dimensions of the rotating disk used for experimental testing. The longitudinal length of 100 mm and transversal width of 60 mm for region 4 (yoke) are shorter than corresponding values in region 2. However, the dimensions of the region 4 are considered identical to region 4 in order to solve analytically the computational model with less complexity and minimum deficiency of accuracy. For example, similar approximations are used for analytical modeling of linear induction machines with consideration of primary dimensions identical as secondary, which show outstanding accuracy for the performance analysis of linear induction machines [28]-[29].

MATLAB program is used to implement analytical method for performance analysis and parametric calculations of the eddy current speed sensor. Fig. 4 shows a 2D view of the coils and the magnetic flux distribution with iron and aluminum moving parts with the magnetic gap between the coils and the moving part, g_m = 6 mm at +16.7 m/s and 800 Hz. The magnetic flux distributions are drawn using contour plot of equi-value for A_z in (5) at z = 0 (mid-plane of the sensor, *y*-*x*) in MATLAB where A_x = 0 due to the symmetry. The conductivities of iron and aluminum are σ_m = 6 MS/m and 33.5 MS/m, respectively. The relative permeability of the iron moving part is estimated as $\mu_{r,m}$ =100 for the initial calculations [24]. The magnetic yoke is a silicon steel lamination with relative permeability $\mu_{r,y}$ =1000 and conductivity σ_y = 3.14 MS/m. The influence of finite lengths for magnetic yoke can be neglected as magnetic flux is more concentrated in the vicinity of the excitation coils as shown in Fig. 4, which has shorter length than yoke. The eddy current distributions on the surface of the iron and aluminum moving parts at +16.7 m/s and 800 Hz are depicted in Fig. 5. They are drawn using contour plot of equi-value for streamline function, F_y obtained from current density, J at y = 0 (*z*-*x* plane).

$$\nabla \cdot \vec{J} = 0 \;\rightarrow \vec{J} = \nabla \times \vec{F}, \qquad F = (0, F_y, 0)$$
$$F_y = -\int J_{x,2} \cdot dz$$
$$F_y = \int J_{z,2} \cdot dx$$
$$J_{z,2} = -\sigma_m j(\omega - V \cdot p) \cdot A_{z,2}$$
$$J_{x,2} = -\sigma_m j(\omega - V \cdot p) \cdot A_{x,2} \quad (14)$$

Final version of this paper was published at
IEEE Transactions on Industry Applications. 2022, 2022 7847-7856 DOI: 10.1109/TIA.2022.3198625

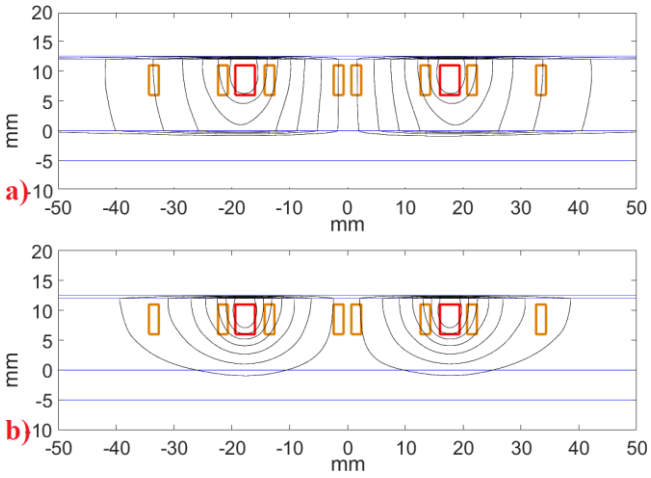

Fig. 4. The magnetic flux distribution in the eddy current speed sensor with a magnetic yoke in the *y*-*x* plane (*z*=0) at +16.7 m/s and 800 Hz, a) iron moving part, b) aluminum moving part

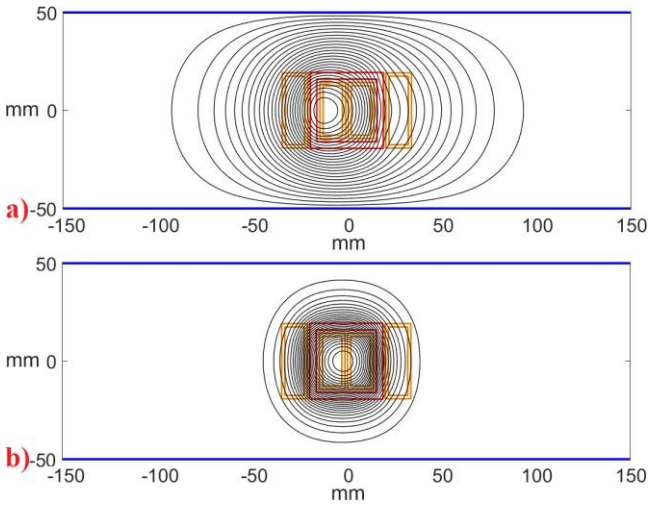

Fig. 5. The eddy current distribution on the surface of the moving part with a magnetic yoke in the *z*-*x* plane (*y*=0) at +16.7 m/s and 800 Hz, a) iron moving part, b) aluminum moving part

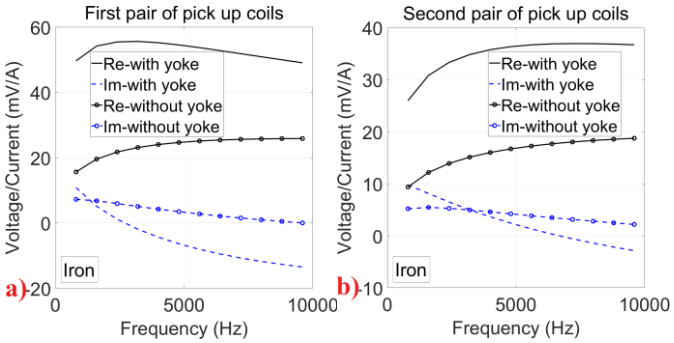

Fig. 6. The real (Re) and imaginary (Im) components of the induced voltage per applied current versus frequency with and without magnetic yokes for an iron moving part at +16.7 m/s and g_m= 6 mm – a) first pair and b) second pair of pick-up coils

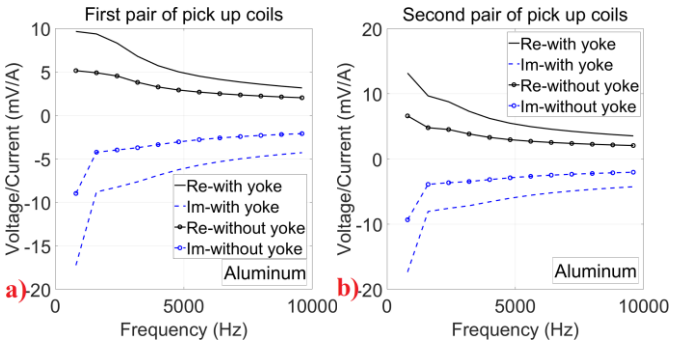

Fig. 7. The real (Re) and imaginary (Im) components of induced voltage per applied current versus frequency with and without magnetic yokes for an aluminum moving part at +16.7 m/s and g_m= 6 mm – a) first pair and b) second pair of pick-up coils

B. Parametric Analysis of The Sensor

Fig. 6 and Fig. 7 show the real (U_r) and imaginary (U_i) components of voltages to current ratios versus frequency up to 10 kHz for the first and second pairs of pick-up coils at +16.7 m/s. The real and imaginary components of the voltages are calculated with the excitation coil current considered as a reference signal. Using a magnetic yoke significantly increases the sensitivity of the sensor.

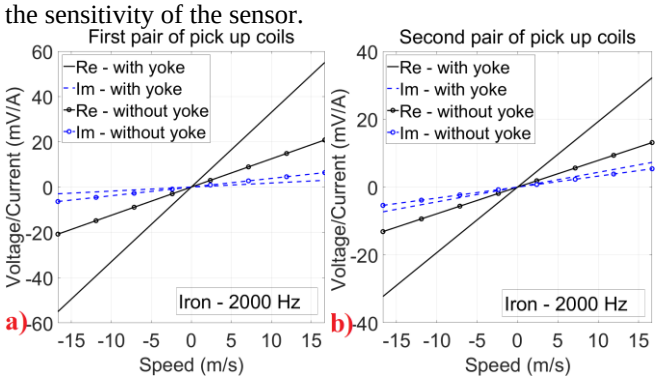

Fig. 8. The real (Re) and imaginary (Im) components of the induced voltage per applied current versus speed with and without magnetic yokes for an iron moving part at 2000 Hz and g_m= 6 mm – a) first pair and b) second pair of pick-up coils

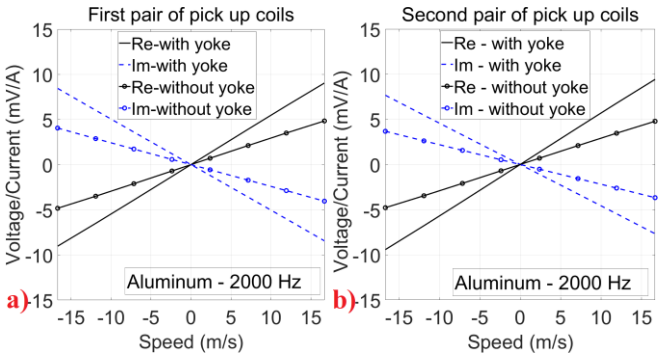

Fig. 9. The real (Re) and imaginary (Im) components of the induced voltage per applied current versus speed with and without magnetic yokes for an aluminum moving part at 2000 Hz – g_m= 6 mm – a) first pair and b) second pair of pick-up coils

The real and imaginary components of the induced voltages decrease monotonically with increasing frequency for an aluminum moving part. This is caused by the decreasing magnetic

Final version of this paper was published at
IEEE Transactions on Industry Applications. 2022, 2022 7847-7856 DOI: 10.1109/TIA.2022.3198625

flux penetration in nonmagnetic aluminum. However, the curves of the real and imaginary components of the induced voltages versus frequency show different trends for a magnetic iron moving part, because of the higher relative magnetic permeability.

The real and imaginary components of the induced voltage curves versus speed show high linearity in Fig. 8 and Fig. 9 up to ±16.7 m/s. This depicts the suitability of the eddy current sensor for use as a speed and velocity meter. The polarity of the voltage changes with the speed direction.

The first pair of pick-up coils has higher induced voltage and sensitivity versus speed. However, the second pair of pick-up coils also shows comparable sensitivity. Using two pairs of pick-up coils helps to increase the fault-tolerant capability of the sensor and the lift-off compensation or temperature compensation of the conductive moving part. The temperature of the conductive moving part changes the material properties in terms of relative magnetic permeability and electrical conductivity, which affect the performance of the eddy current sensor [23]. The relative permeability of the iron moving part has a high impact on the performance of the sensor. Decreasing the relative magnetic permeability increases the sensitivity of the sensor, because the magnetic penetration depth in the moving part is greater for lower relative permeability [24].

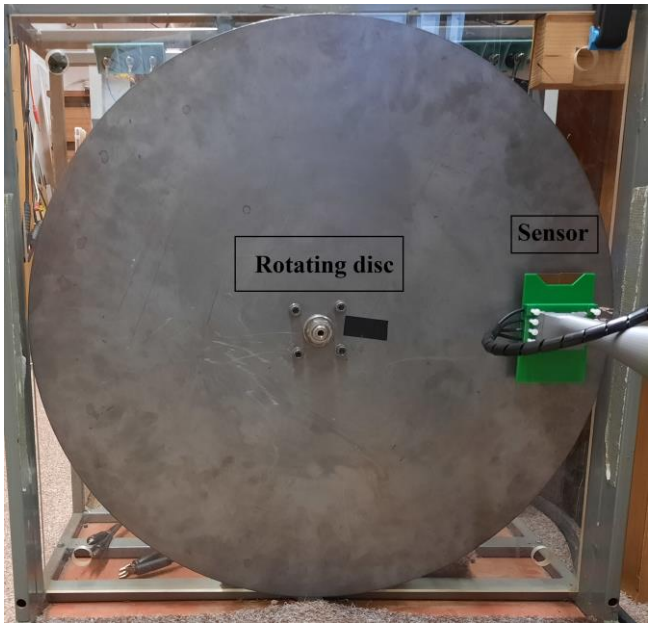

Fig. 10. Eddy current speed sensor with a rotating disk

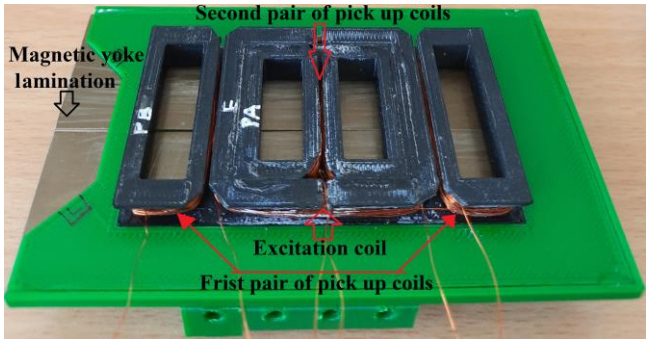

Fig. 11. The coils and magnetic yoke in eddy current speed sensor

IV. Sensor Measurements

Fig. 10 and Fig. show the experiment elements, rotating disk and the eddy current linear speed sensor. The moving part is a rotating disk with a 55.5 cm external diameter. The center of the speed sensor is located at a distance of r_{ds}=22.75 cm from the center of the disk. As shown in Fig. 1, the dimensions of the speed sensor are sufficiently smaller than the rotating disk to model accurately the relative linear motion between the sensor and the moving part in the measurements. Each pair of antiserially connected pick up coils are connected to lock-in amplifier, Stanford Research System, model SR830 DSP, which is used for measurements of the real and imaginary components of the induced voltages of the pick-up coils. The excitation coil with resistance 20.78 Ω in series with external resistance 9.02 Ω are connected to a signal generator with internal resistance 50 Ω and voltage amplitude 10 V. The voltage across the external resistance is used to measure the current in the excitation coil. The rms value of the measured current at different gaps, g_m and various excitation frequencies are presented in Table II and Table III with and without yokes. The real and imaginary components of the induced voltages are measured relative to the excitation coil current as a reference signal.

TABLE II
Measured Current with and without Magnetic Yoke

g_m= 6 mm		800 Hz	2000 Hz	10000 Hz
Iron	no-yoke	86.6 mA	79.2 mA	36.7 mA
	yoke	83.8 mA	70.9 mA	28.2 mA
Aluminum	no-yoke	87.5 mA	83.0 mA	44.1 mA
	yoke	86.3 mA	79.3 mA	36.5 mA

TABLE III
Measured Current with and without Magnetic Yoke

g_m= 8 mm		800 Hz	2000 Hz	10000 Hz
Iron	no-yoke	87.0 mA	80.1 mA	37.3 mA
	yoke	84.4 mA	72.0 mA	28.6 mA
Aluminum	no-yoke	87.6 mA	82.9 mA	42.5 mA
	yoke	86.3 mA	78.6 mA	34.5 mA

A. Experimental Results of The Sensor

The experimental results concerning differential voltages for the first and second pairs of pick-up coils with iron and aluminum moving parts and with a magnetic yoke are shown in Fig. 12 and Fig. 13 at excitation frequencies of 800 Hz and 2 kHz. As shown in Fig. 12, the linearity of the voltage versus speed curve is smaller at 800 Hz for an aluminum moving part above 10 m/s.

Final version of this paper was published at
IEEE Transactions on Industry Applications. 2022, 2022 7847-7856 DOI: 10.1109/TIA.2022.3198625

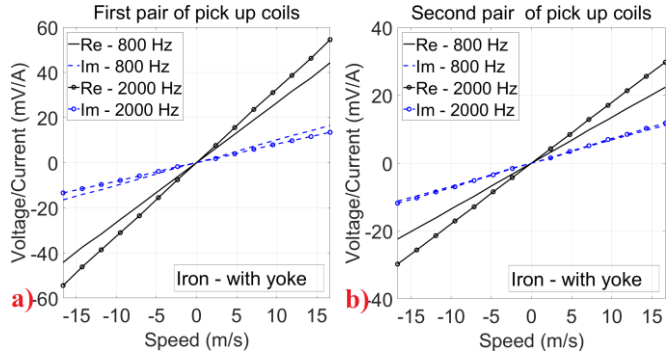

Fig. 12. The real (Re) and imaginary (Im) components of the induced voltage per applied current versus speed with a magnetic yoke for an iron moving part for g_m= 6 mm – a) first pair and b) second pair of pick-up coils

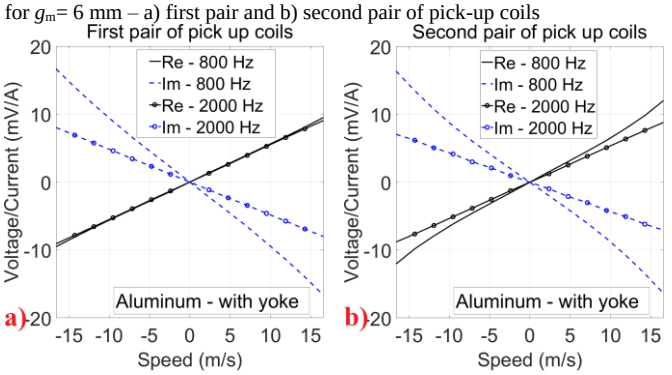

Fig. 13. The real (Re) and imaginary (Im) components of the induced voltage per applied current versus speed with a magnetic yoke for an aluminum moving part for g_m= 6 mm – a) first pair and b) second pair of pick-up coils

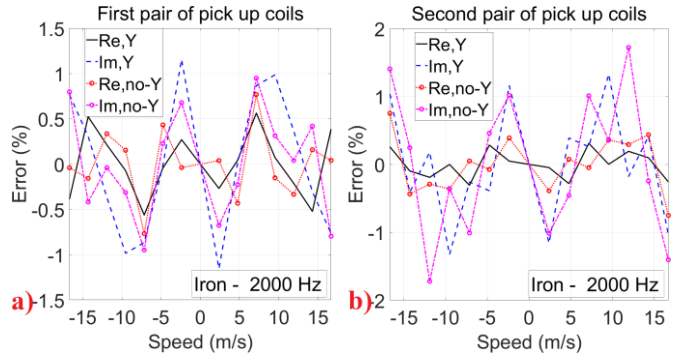

Fig. 14. The measured nonlinearity error of the real value (Re) and the imaginary value (Im) of the induced voltage per applied current versus speed with (Y) and without (no-Y) a magnetic yoke for an iron moving part for g_m= 6 mm – a) first pair and b) second pair of pick-up coils

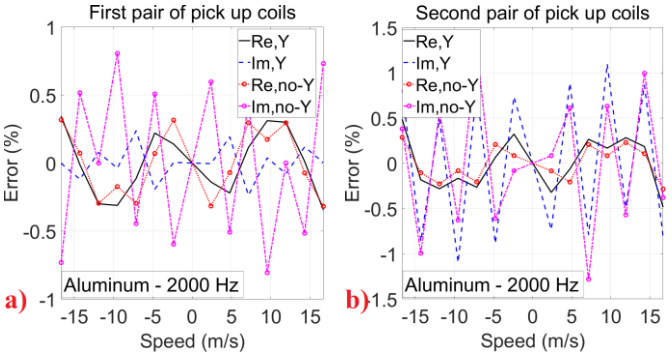

Fig. 15. The measured nonlinearity error of the real value (Re) and the imaginary value (Im) of the induced voltage per applied current versus speed with (Y) and without (no-Y) a magnetic yoke for an aluminum moving part for g_m= 6 mm – a) first pair and b) second pair of pick-up coils

As shown in Fig. 14 and Fig. 15, the nonlinearity error can be brought down as low as 0.3%, for the first and second pairs of pick-up coils. The measured sensitivity, K_r, corresponding to the real component of the voltage, U_r=$K_r \cdot V \cdot I$, and the measured sensitivity, K_i, corresponding to the imaginary component of the voltage, U_i=$K_i \cdot V \cdot I$ per applied current, I, are presented in Table IV – Table VII at 2 kHz and 10 kHz for iron and aluminum moving parts with gaps of 6 mm and 8 mm. For an iron moving part, the ratio of the real component sensitivity, K_r, to the imaginary component sensitivity, K_i, is 2 to 20 times higher with a magnetic yoke than without a magnetic yoke. There are different trends for an aluminum moving part, with a smaller difference when there is a magnetic yoke. The polarity of the imaginary component of the voltage and its sensitivity become negative for an aluminum moving part. Increasing the gap, g_m, from 6 mm to 8 mm (+33%) reduces by about 20% to 30% the real component of the induced voltage for an iron moving part. This decrease is smaller for an aluminum moving part, especially at higher frequencies.

A compact synchronous detector could be used to measure the real and imaginary components of the voltage in the eddy current speed sensor. The measured voltages are converted to the speed values and speed polarities using sensitivities values in Table IV – Table VII with consideration of excitation coil current. The outstanding linearity of the dependence of real and imaginary components of sensor output voltage versus speed as shown in Fig. 12 and Fig. 13 results in the same linearity characteristics for the dependence of absolute value of the voltage, U_a $\left(=\sqrt{U_r^2+U_i^2}\right)$ versus speed. Therefore, a voltmeter can be used to read rms value of the sensor voltage to measure the speed value when absolute value of the voltage is only readable. A phase sensitive detector can be utilized to sense the polarity of speed as for LVDT sensors.

TABLE IV
SENSITIVITY OF AN EDDY CURRENT SENSOR FOR AN IRON MOVING PART – FIRST PAIR OF PICK-UP COILS

Sensitivity mV/(A·m/s)	with yoke		without yoke	
	Real	Imaginary	Real	Imaginary
g_m = 6 mm f = 2000 Hz	3.252	0.8109	1.178	0.5266
g_m = 6 mm f = 10000 Hz	3.204	- 0.3886	1.607	0.228
g_m = 8 mm f = 2000 Hz	2.448	0.6197	0.9331	0.4085
g_m = 8 mm f = 10000 Hz	2.461	- 0.22	1.255	0.1924

TABLE V
SENSITIVITY OF AN EDDY CURRENT SENSOR FOR AN IRON MOVING PART – SECOND PAIR OF PICK-UP COILS

Sensitivity mV/(A·m/s)	with yoke		without yoke	
	Real	Imaginary	Real	Imaginary
g_m = 6 mm f = 2000 Hz	1.789	0.7143	0.7161	0.3801
g_m = 6 mm f = 10000 Hz	2.277	0.1065	1.081	0.235
g_m = 8 mm f = 2000 Hz	1.279	0.5055	0.539	0.2871

Final version of this paper was published at
IEEE Transactions on Industry Applications. 2022, 2022 7847-7856 DOI: 10.1109/TIA.2022.3198625

g_m = 8 mm f = 10000 Hz	1.638	0.1022	0.8277	0.2091

TABLE VI
SENSITIVITY OF AN EDDY CURRENT SENSOR FOR AN ALUMINUM MOVING PART – FIRST PAIR OF PICK-UP COILS

Sensitivity mV/(A·m/s)	with yoke		without yoke	
	Real	Imaginary	Real	Imaginary
g_m = 6 mm f = 2000 Hz	0.5482	- 0.4829	0.2958	- 0.244
g_m = 6 mm f = 10000 Hz	0.199	- 0.2198	0.1214	- 0.1145
g_m = 8 mm f = 2000 Hz	0.4822	- 0.3912	0.2651	- 0.1841
g_m = 8 mm f = 10000 Hz	0.1605	- 0.2156	0.1151	- 0.1058

TABLE VII
SENSITIVITY OF AN EDDY CURRENT SENSOR FOR AN ALUMINUM MOVING PART – SECOND PAIR OF PICK-UP COILS

Sensitivity mV/(A·m/s)	with yoke		without yoke	
	Real	Imaginary	Real	Imaginary
g_m = 6 mm f = 2000 Hz	0.5329	- 0.4282	0.2703	- 0.2097
g_m = 6 mm f = 10000 Hz	0.1943	- 0.22	0.1075	- 0.1036
g_m = 8 mm f = 2000 Hz	0.4339	- 0.3099	0.2266	- 0.1466
g_m = 8 mm f = 10000 Hz	0.1664	- 0.1849	0.1025	- 0.09522

B. Comparison between The Analytical Results and The Experimental Results of The Sensor

Fig. 16 and Fig. 17 compare the experimental and analytical results for the absolute component of the voltage. The analytical results coincide well with the experimental results. This shows the appropriateness of the 3D analytical method for further design and optimization of an eddy current speed sensor and higher-speed operation. The 3D analytical method could therefore also be used for evaluating the sensor in higher speed ranges and at higher frequencies.

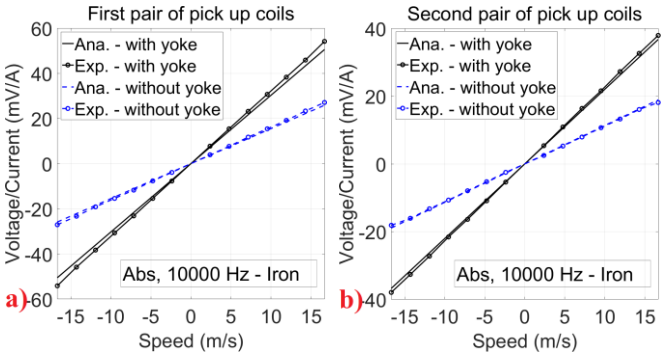

Fig. 16. The comparison between the experimental (Exp.) and analytical (Ana.) results for the absolute value (Abs) of the induced voltage per applied current versus speed, with and without a magnetic yoke, for an iron moving part for g_m= 6 mm – a) first pair and b) second pair of pick-up coils

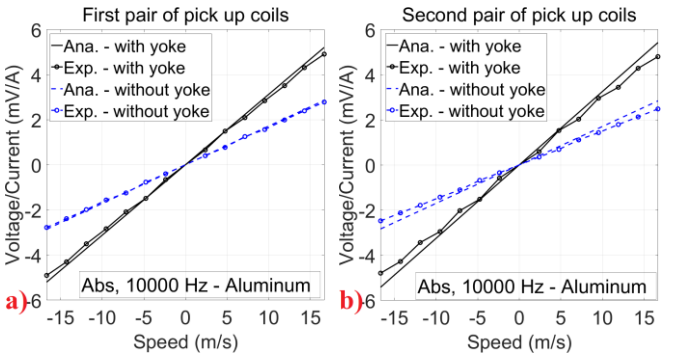

Fig. 17. A comparison between the experimental results (Exp.) and the analytical results (Ana.) for the absolute value (Abs) of the induced voltage per applied current versus speed with and without a magnetic yoke for an aluminum moving part for g_m= 6 mm – a) first pair b) second pair of pick-up coils

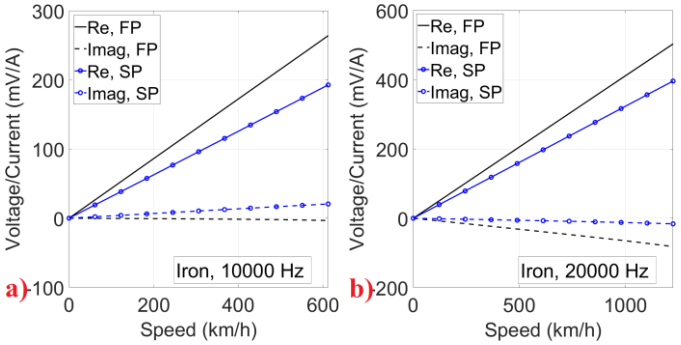

Fig. 18. – The voltage results for first (FP) and second (SP) pairs of pick-up coils for an iron moving part without a magnetic yoke using analytical method - a) up to 612.5 km/h, 10 kHz, b) up to 1225 km/h, 20 kHz

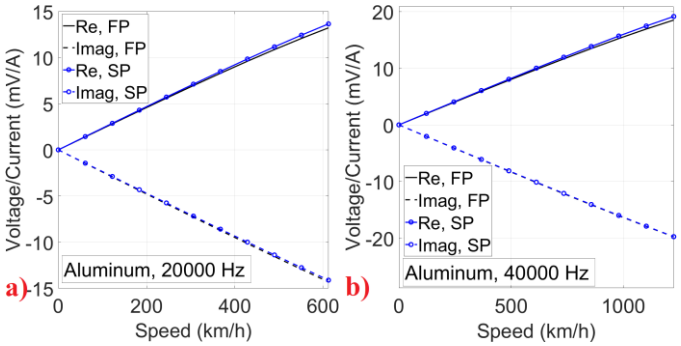

Fig. 19. - The voltage results for the first (FP) and second (SP) pairs of pick-up coils for an aluminum moving part without a magnetic yoke using analytical method - a) up to 612.5 km/h, 10 kHz, b) up to 1225 km/h, 20 kHz

V. OPERATION OF THE SENSOR AT HIGHER SPEEDS

The low-speed range can be considered below 15 m/s (54 km/h) to 20 m/s (72 km/h) and upper speeds can be considered in high-speed range for linear induction devices, such as linear induction machines [30]. Fig. 18 and Fig. 19 show the voltage results calculated using analytical method of an eddy current speed sensor without a magnetic yoke up to 1225 km/h (340 m/s), which can be considered as the theoretical maximum speed of Hyperloop [14]-[15]. The possible maximum excitation frequency is selected to achieve an optimum compromise between the highest sensitivity and the lowest nonlinearity error. The optimum excitation frequencies

Final version of this paper was published at
IEEE Transactions on Industry Applications. 2022, 2022 7847-7856 DOI: 10.1109/TIA.2022.3198625

for the iron moving part are 10 kHz and 20 kHz for a maximum speed of 612.5 km/h and 1225 km/h, respectively. The optimum excitation frequencies for an aluminum moving part are 20 kHz and 40 kHz, respectively. The sensitivity of the eddy current speed sensor decreases more for an aluminum moving part at higher frequencies, than for an iron moving part, which does not change considerably. Operating the eddy current speed sensor at high frequencies to achieve high linearity is technically preferable without a magnetic yoke, despite its lower sensitivity. The reason is that the self-inductance of the excitation coil and its corresponding reactance voltage drop are lower, and a smaller voltage source is therefore required for the excitation coil to achieve the same current.

VI. Discussions

The implementation of the second pair of pick-up coils in the eddy current speed sensor with the same sensitivity as the first pair of pick-up coils increases the reliability of the sensor. It makes the sensor more fault tolerant, and it can also be used for liftoff and temperature compensation. A novel method for implementing the second coil pair inside the excitation coil helps to make optimal use of the sensor space and to enhance the performance of the sensor.

At present, complicated structures can be easily modeled in 3D FEM. However, 3D time stepping FEM with consideration of motion and skin effect is very time consuming due to the large numbers of required mesh nodes. Therefore, it is not a time efficient method for parametric analysis and design optimization. Modeling of movement in 3D FEM causes numerical errors due to the mesh movement, which affects the accuracy of calculated voltage in eddy current speed sensor [23]-[25]. The proposed novel 3D analytical method shows excellent accuracy and time efficient simulations despite its simple approach for the modeling of eddy current speed sensor. The transformer component of eddy current caused by AC fields and motional component of eddy current caused by relative motion of excitation coil and moving object were modeled in the 3D analytical model. And exact dimensions of the rectangular coils are considered and the induced voltages in the pick up coils are exactly calculated.

Tachometers, optical and Hall effect speed sensors are commercially available for railway applications. They indirectly measure linear speed, and they are usually installed or coupled in the vicinity of traction motors, gearboxes and wheels axis for railway applications. For example, Hall effect speed sensors utilize magnetic ring with permanent magnets or toothed ring with variable reluctance gear coupled to the rotating parts, which they have high reliability, appropriate robustness and fault-tolerant capability to work for different industrial applications [31]. They show superior performance in comparison with optical speed sensors because they are more cost effective and less sensitive to the damages and mechanical faults. Substantial errors for indirect speed measurement can be caused by the wheel slip and slide, for example, in rainy weather. These errors can be avoided by using direct speed measurement method with eddy current speed sensors.

An eddy current speed sensor utilizing the fluxgate effect in an amorphous ring core was presented in [32], which measures the field of motional eddy current in the moving conductive objects and coverts to speed values. This is a rather complicated sensor with a high linearity error of approximately 5 %. A Hall effect eddy current speed sensor using permanent magnet excitation, which shows poor offset stability, was presented in [33]. The eddy current speed sensors presented in [22] and [32]-[33] were only operated with aluminum moving parts.

A single-chip synchronous detector, e.g., the AD630 modulator/demodulator IC, can be used for the processing the output voltage with reasonable cost, instead of the lock-in amplifier. The structure of the sensor is simple, as it only consists of rectangular coils and steel lamination or ferrite yoke. Therefore, the eddy current speed sensor with its signal processing unit could be a cost-effective option for the linear speed measurement. Its cost effective and simple configuration is a vital advantage over commercial speed sensors.

VII. Conclusion

A novel parallel type of eddy current speed sensor has been designed, analyzed and tested. A novel 3D analytical method was used for sensor modelling. The analytical results coincide well with the results of measurements, and they prove the suitability of the proposed eddy current sensor for linear speed measurements.

Extracting the real and imaginary components of the pick-up coils using a lock-in amplifier has advantages over using the absolute value of the voltage: 1 - A real component or an imaginary component can have a smaller nonlinearity error than the absolute value of the voltage, as shown in the results. 2 - Either a real component or an imaginary component can be used for error compensation if the other component is used as a speed meter.

It is a standard method to consider using auxiliary sensors beside the main sensor for error compensation. The second pair of pick-up coils helps to increase the degree of freedom to compensate the lift-off error, or the error caused by a change in the temperature of the moving part. The voltages of the second pair of pick-up coils are at the same level as the voltages of the first pick-up coils, which can be utilized for error compensation. Further mechanical and thermal effects can be compensated by adding extra pick-up coils. The use of double frequency or multiple frequency signals for excitation is an alternative method for error compensation. For example, the voltage corresponding to one frequency can be considered as a speed meter and the other voltages can be utilized for compensation.

The operation of the eddy current speed sensor without a magnetic yoke was analytically analyzed for higher speeds up to 1225 km/h. The low sensitivity of the aluminum part can be compensated by increasing the number of turns and the dimensions of the excitation coil and pick-up coils. A 0.5 mm silicon steel lamination was used for the magnetic yoke; it can be replaced by a ferrite core, which allows higher excitation frequencies, but it is fragile. Another option is to use a nanocrystalline material.

Final version of this paper was published at
IEEE Transactions on Industry Applications. 2022, 2022 7847-7856 DOI: 10.1109/TIA.2022.3198625

REFERENCES

[1] M. Mirzaei, P. Ripka, and V. Grim, "A novel eddy current speed sensor with a Ferrite E-core," *13th International Symposium on Linear Drives for Industry Applications (LDIA)*, Wuhan, China, 1-3 July 2021

[2] Speed Sensors, https://www.te.com/usa-en/products/sensors/speed-sensors.html?tab=pgp-story

[3] A. Accetta, M. C. Di Piazza, M. Luna, and M. Pucci, "Electrical losses minimization of linear induction motors considering the dynamic end-effects," *IEEE Trans. Industry Applications*, vol. 55, no. 2, pp. 1561-1573, March/April 2019

[4] D. Hu, W. Xu, R. Dian, and Y. Liu, "Loss minimization control strategy for linear induction machine in urban transit considering normal force," *IEEE Trans. Industry Applications*, vol. 55, no. 2, pp. 1536-1549, March/April 2019

[5] L. Du, Q. Sun, J. Bai, X. Wang, and T. Xu, "Speed calibration and traceability for train-borne 24 GHz continuous-wave doppler radar sensor," *Sensors*, vol. 20, 2020, Art. no.1230.

[6] J. Otegui, A. Bahillo, I. Lopetegi, and L. Enrique Diez, "A survey of train positioning solutions," *IEEE Sensors Journal*, vol. 17, no. 20, pp. 6788-6797, October 15, 2017

[7] T. Strauss, C. Hasberg, S. Hensel, "Correlation based velocity estimation during acceleration phases with application in rail vehicles," *2009 IEEE/SP 15th Workshop on Statistical Signal Processing*, pp.721-724, Sept. 2009

[8] S. Hensel, C. Hasberg, and C. Stiller, "Probabilistic rail vehicle localization with eddy current sensors in topological maps," *IEEE Trans. intelligent Transportation Systems*, vol. 12, no. 4, pp. 1525-1536, Dec. 2011

[9] S. Hensel, T. Strauss, M. Marinov, "Eddy current sensor based velocity and distance estimation in rail vehicles," *IET Science, Measurement & Technology*, vol. 9, no. 7, pp. 875–881, 2015

[10] L. Sun, J. Taylor, A. D. Callegaro, and A. Emadi, "Stator-PM-based variable reluctance resolver with advantage of motional back-EMF," *IEEE Trans. Ind. Electronics.* vol. 67, no. 11, pp. 9790-9801, Nov. 2020

[11] P. Peralta, S. Thomas, and Y. Perriard, "Characterization and verification of eddy-current position sensing for magnetic levitation," *IEEE Trans. Industry Applications*, vol. 57, no. 6, pp. 5796-5805, Nov./Dec. 2021

[12] T. Konig, T. Greiner, A. Zern, Z. Kantor, A. Szabo, and A. Hetznecker, "Using eddy currents within magnetostrictive position sensors for velocity estimation," *IEEE Sensors Journal*, vol. 19, no. 15, pp. 6325-6334, August 1, 2019

[13] J. Liu, T. A. Nondahl, J. Dai, S. Royak, and P. B. Schmidt, "A seamless transition scheme of position sensorless control in industrial permanent magnet motor drives with output filter and transformer for oil pump applications," *IEEE Trans. Industry Applications*, vol. 56, no. 3 pp. 2180-2189, May/June 2020

[14] D. Tudor, and M. Paolone, "Optimal design of the propulsion system of a hyperloop capsule," *IEEE Transactions on Transportation Electrification*, vol. 5, no. 4, pp. 1406-1418, 2019

[15] W-Y Ji, G. Jeong, C.-B. Park, I.-H. Jo, and H.-W. Lee, "A study of non-symmetric Double-Sided Linear Induction Motor for Hyperloop All-In-One System (Propulsion, Levitation, and Guidance)," *IEEE Transactions on Magnetics*, vol. 54, no. 11, 2018

[16] W. Xu, X. Xiao, G. Du, D. Hu, and J. Zou, "Comprehensive efficiency optimization of linear induction motors for urban transit," *IEEE Transactions on Vehicular Technology*, vol. 69, no. 1, pp. 131-139, Jan 2020

[17] C. Gong, A. Tuysuz, M. Flankl, T. Stolz, J. Kolar, and T. Habetler "Experimental analysis and optimization of a contactless eddy-current based speed sensor for smooth conductive surfaces," *IEEE Transactions on Industrial Electronics*, vol. 67, no. 2, pp. 8817 - 8828, Oct 2020

[18] T. C. Wang, "Linear induction motor for high-speed ground transportation," *IEEE Transactions on Industry and General Applications*, vol. IGA-7, no. 5, pp. 632-642, Sept 1971

[19] T. A. Nondahl, and D. W. Novotny, "Pole-by-pole model of a linear induction machine using conformal mapping coefficients," *IEEE Transactions on Power Apparatus and Systems*, vol. 98, no. 4, pp. 1345 - 1353, July 1979

[20] Q. Lu, L. Li, J. Zhan, X. Huang, and J. Cai, "Design optimization and performance investigation of novel linear induction motors with two kinds of secondaries," *IEEE Trans. Industry Applications*, vol. 55, no. 6, pp. 5830-5842, No./Dec. 2019

[21] R. Andre, H. de Oliveira, R. M. Stephan, A. C. Ferreira, and J. Murta-Pina, "Design and innovative test of a linear induction motor for urban MagLev vehicles," *IEEE Trans. Industry Applications*, vol. 56, no. 6., pp. 6949-6956, Nov./Dec. 2020

[22] N. Takehira and A. Tanaka, "Analysis of a perpendicular-type eddy-current speed meter," *IEE Proceedings A (Physical Science, Measurement and Instrumentation, Management and Education, Reviews)*, vol.135, no.2, pp. 89-94, Feb 1988.

[23] M. Mirzaei, P. Ripka, A. Chirtsov, J. Vyhnanek, and V. Grim, "Design and modeling of a linear speed sensor with a flat type structure and air coils," *Journal of Magnetism and Magnetic Materials*, vol. 495, 165834, 1 February 2020

[24] M. Mirzaei, P. Ripka, A. Chirtsov, and V. Grim, "Eddy current speed sensor with magnetic shielding," *Journal of Magnetism and Magnetic Materials*, vol.502, 166568, May 2020.

[25] M. Mirzaei, P. Ripka, and V. Grim, "A novel eddy current speed sensor with a Ferrite E-core," *IEEE Magnetics Letters* , vol. 11, 8102905, 08 May 2020

[26] M. Mirzaei, and P. Ripka, "A linear eddy current speed sensor with a perpendicular coils configuration," *IEEE Transactions on Vehicular Technology*, vol. 70, no. 4, pp. 3197 - 3207, April 2021

[27] K.J. Binns, P.J. Lawrenson, and C.W. Trowbridge, *The Analytical and Numerical Solutions of Electric and Magnetic Fields*, Published by John Wiley & Sons Ltd., 1992

[28] S. Yamamura, H. Ito, and Y. Ishulawa, "Theories of the linear induction motor and compensated linear induction motor," *IEEE Trans. Power Apparatus and Systems*, vol. PAS-91, no. 4, pp.1700 - 1710, 1972

[29] K. Yoshida and S. Nonaka, "Levitation forces in single-sided linear induction motors for high-speed ground transport," *IEEE Trans. Mag.*, vol. 11, no. 6, pp. 1717-1719, 1975

[30] S. Yamamura, *Theory of Linear Induction Motors*, John Wiley & Sons Inc, 2nd edition, Tokyo, 1979

[31] P. D. Shilovskikh and I. I. Rastvorova, "Analysis of the dependence between air gap size on the output signal of Hall effect speed sensors," *2022 Conference of Russian Young Researchers in Electrical and Electronic Engineering (ElConRus)*, Saint Petersburg, Russian Federation, 2022

[32] T. Sonoda, R. Ueda, K. Fujitani, T. Irisa, and S. Tatata, "DC magnetic field type eddy current speed sensor detecting cross magnetization field with amorphous core", *IEEE Trans. Magn.*, vol. MAG-21, no. 5, pp. 1732-1734, Sep. 1985

[33] E. Cardelli, A. Faba, and F. Tissi, "Contact-less speed probe based on eddy currents," IEEE Trans. Magn., vol. 49, no. 7, pp. 3897–3900, Jul. 2013.